

## **Recent Achievements for In-situ Measurement: Applications to an Actual Decommissioning Project**

F. Lamadie, P. Gironès, C. Le Goaller, C. Mahé  
Commissariat à l'Énergie Atomique (CEA) Marcoule Research Center  
Direction de l'Énergie Nucléaire, Département de Déclassement et de Conduite des Opérations,  
BP 17171, 30207 Bagnols-sur-Cèze Cedex  
France

J.Y. Kohler, M.A. Risser  
Commissariat à l'Énergie Atomique (CEA) Marcoule Research Center  
Direction des Applications Militaires, Département Projet et Ingénierie des Installations,  
BP 17171, 30207 Bagnols-sur-Cèze Cedex  
France

### **ABSTRACT**

Decommissioning a nuclear facility implies a policy of limiting the waste volume and its chemical—and especially radiological—toxicity. It is therefore important to determine the activity level contained in each component that will be dismantled. A variety of methods and analysis techniques are used for this purpose, ranging from simple dose rate measurements to  $\gamma$  spectrometry and  $\gamma$  imaging. The results of several measurement campaigns in a reactor currently in operation but for which decommissioning studies have now been undertaken are discussed. The measurements provide additional radiological data for the waste inventory, which is one of the first issues to be examined. This discussion focuses on the methods used ( $\gamma$  imaging, *in situ*  $\gamma$  spectrometry, etc.), the results obtained, and their implications for the project, as well as the technological and methodological innovations implemented during these campaigns.

### **INTRODUCTION**

All the actions described in this document concern the project feasibility studies undertaken by the *Commissariat à l'Énergie Atomique* (CEA) for decommissioning a reactor at the Marcoule nuclear site. The objective is to validate quantity and activity level of long-lived intermediate-level waste (LL-ILW), most of which will comprise metal components activated after extended exposure to the neutron flux in the core. The two main sources of LL-ILW will be the reactor vessel and the core internals (control rods, guide tubes, etc.). Under French legislation, waste is classified according to its specific activity and half-life. Although disposition routes are operational for some wasteforms, others—including LL-ILW—are placed in interim storage pending the availability of viable technical solutions.

The reactor vessel is critical for determining the scope of the waste management plan. It is the massive component (20 metric tons) subject to the greatest activation during operation and thus constitutes the major source of LL-ILW, hence the importance of accurately evaluating its specific activity at every point. The activity cannot be analyzed by destructive measurements on samples taken from the reactors, which are still in operation. The selected method combines theoretical activation calculations and *in situ* measurements. The combination of modeling and

activation calculations provided an exhaustive and relatively reliable waste balance inventory including the activity levels of the relevant radioelements. The inventory quantified the pure  $\beta$  emitters ( $^{59}\text{Ni}$ ,  $^{63}\text{Ni}$ , etc.), which in this case are the design basis elements for waste management purposes. The validity of the models was confirmed by comparing the measured and predicted activities for selected  $\beta\gamma$  emitters. The methods employed to obtain these results are described in the first section on characterizing the reactor vessel.

The reactor internals represent a smaller waste volume than the reactor vessel (9 metric tons), but also potentially constitute long-lived intermediate-level waste. Unlike the reactor vessel, they can be handled and removed from the core for more thorough characterization. Destructive measurements were also carried out on old internal components, and several nondestructive measurement techniques ( $\gamma$  imaging, high and low resolution  $\gamma$  spectrometry) were also used to obtain as much information as possible. As with the reactor vessel, the purpose of the measurements was to validate the results calculated using the models. These measurements are discussed in the second section on characterizing the internal components.

Both characterization campaigns were based on specific nondestructive measurement techniques. Several recently developed methods were used; three of these are detailed in the third section.

## CHARACTERIZING THE REACTOR VESSEL

The objective was to determine as accurately as possible the  $\beta\gamma$ -emitter profile and activation level vertically along the reactor vessel as a means to specify the cutting pattern to optimize waste management. The measurement conditions were difficult for three reasons: access to the vessel was possible only via a manhole 70 cm in diameter in the reactor slab, limiting the size of the detection equipment; moreover, all the data were acquired underwater, inside the reactor thermal protection vessel, requiring the use of a reliable, leaktight system; and finally, several internal components in the core were liable to influence the measurement results.

A detector carrier and a suitable measurement strategy were developed to meet these constraints. The carrier was designed around three main functions. First, to provide access to the vessel wall.: This function was ensured by a combination of mechanisms and handling equipment. The detection head can move up and down, pivot around its centerline, and move radially toward the measurement surface, with all motion controlled from the reactor slab. Second, to collimate the detector. This function is ensured by a lead cylinder 270 mm in diameter, 240 mm high, and weighing about 155 kg surrounding the detector. The cylindrical assembly includes two orifices, one to accommodate a leaktight stainless steel bowl containing the detector, and the other for attaching an air-filled tube. Third, to enhance the  $\gamma$  transmission between the source and detector. This is the role of the air-filled stainless steel tube with tapped ends mounted at right angles to the detection head and in contact with the reactor vessel. The contrast between diffusion in air and water makes it a suitable guide tube for carrying the  $\gamma$  rays to the detector over the preferred path. **Fig. 1** is a three-dimensional view of the detection head [1].

The measurement strategy consisted in acquiring data along two axes, radial and tangential, to allow for the possible influence of the internal components. For better resolution, a  $5\text{ mm}^3$  CdZnTe semiconductor detector ( $6.5 \times 10^{-5}\%$  relative efficiency) corresponding to the expected gamma flux densities (about  $10^6\text{ pH}\cdot\text{s}^{-1}\cdot\text{cm}^{-2}$ ) was used. Measurements were taken at 40 points radially and 13 points tangentially. A single activation product,  $^{60}\text{Co}$ , was identified. The point of

highest activity was detected at level –600 cm, which corresponds to the core midplane. **Table I** shows the results obtained at several characteristic points.

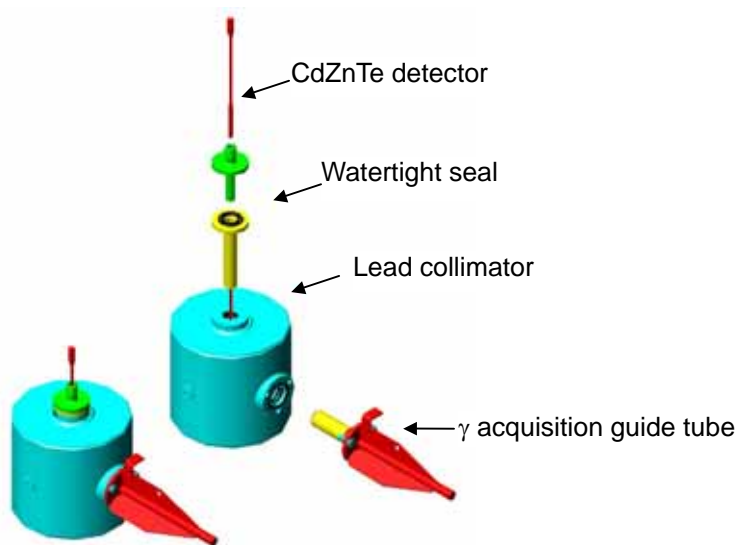


**Fig. 1.** 3D representation of measurement head, with exploded view

**Table I.** Measured activity compared with activity predicted by the model at various levels along the reactor vessel

Reactor elevation (cm)	Activity (GBq·g <sup>-1</sup> )				
	Tangential measurement	Overall uncertainty 2σ	Radial measurement	Overall uncertainty 2σ	Model
420	0.07	16.8%	0.08	18.2%	0.08
445	0.42	16.5%	0.35	12.4%	0.20
495	0.77	16.5%	0.64	12.2%	0.66
598	0.96	16.1%	0.99	12.0%	0.89
610	0.98	16.0%	0.90	12.2%	0.90
660	0.57	16.4%	0.53	12.7%	0.54
700	0.02	19.9%	0.10	13.1%	0.10

The results provide important data for the decommissioning project. They corroborate the activation calculations performed by modeling based on the reactor power history and core models; the agreement between the predicted and measured values is satisfactory, with a maximum discrepancy of less than 25% in the most highly activated zone (the mean difference is less than 15% between level 450 cm and level 700 cm). Although cobalt is a poor indicator, the comparison is possible in this case because the steel grade of the vessel is well known. The ratio between the radial activity and tangential activity is near 1:1, showing that the contribution of core internals is negligible compared with the vessel itself. This is consistent with the model predictions, for which the <sup>60</sup>Co activity of the internals is lower by a factor of 100 than that of the vessel. This corresponds to a difference of about 1%, which would not have been detected by the techniques used (mean uncertainty on the measured values was about 15%).

## CHARACTERIZATION OF CORE INTERNALS

The internals are items inserted in the channels of the reactor tube blocks, and comprise several categories of components. First are the channel tubes that accommodate the control rods together with the mobile devices inserted into the flux (fuel elements and targets intended for irradiation in the core). These items are located in the lower part of the core. The next category includes the control provisions (control, shimming and safety rods), mainly located in the tube block but, depending on their function, also found in the lower part of the core. Plugs at the top of the tube block close the channels and ensure containment and radiological shielding of the reactor loading face. Where possible, each type of in-core object was observed at least once, except for the removable components that are irrelevant to the decommissioning project. In the case of objects considered particularly important for the waste inventory, such as the channel tubes, both peripheral and central items were observed to assess their diversity.

Three measurement techniques were used for characterization purposes: dose rate measurements,  $\gamma$  spectrometry measurements, and  $\gamma$  imaging measurements. The objects were measured in two sequences: first overall with all the detection systems; then in 30 cm steps with the collimated CdZnTe detectors to measure their activation locally.

The data acquisition essentially consisted of collimated CdZnTe measurements ( $\gamma$  scanning) that were then used to calculate the activity. Three probe volumes ( $0.5 \text{ mm}^3$ ,  $5 \text{ mm}^3$  and  $20 \text{ mm}^3$ ) were used to cover the widest possible dynamic range. The irradiation levels in contact with the target objects ranged from a few  $\text{mGy}\cdot\text{h}^{-1}$  to more than a thousand  $\text{Gy}\cdot\text{h}^{-1}$ . The collimator was made of lead with copper lining and sized to record 30 cm segments with a contrast of about 1500 for the 1.33 MeV line of  $^{60}\text{Co}$ . The  $\gamma$  camera images provided an indication of the shape and location of the main radioactive sources, and were taken into account in modeling the objects with a calculation code to estimate their activity. After calibrating the  $\gamma$  camera in an irradiator, the images were also interpreted quantitatively to validate the order of magnitude of the activity values measured with the CdZnTe detectors. GeHP measurements were used for a second qualitative assessment of the activity of the objects by establishing average spectra. This was not possible for the most activated objects due to detector saturation. Ambient dose rate measurements combined with computer models were used to confirm the order of magnitude of the activity values obtained by CdZnTe scanning.

Sixteen items were measured in two campaigns, with 15 measurements for each item. Gamma imaging was performed with the prototype ALADIN camera developed by the CEA [2] using a 4 mm BGO scintillator. **Fig. 2** shows typical images of a fuel element channel tube at the center of the core (dose rate at the camera between 200 and  $650 \text{ mGy}\cdot\text{h}^{-1}$ ).

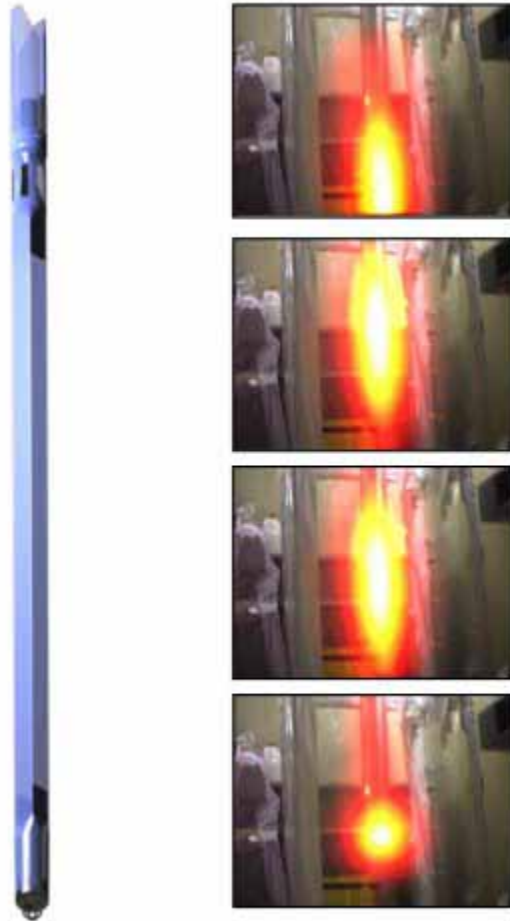


**Fig. 2.**  $\gamma$  imaging examination of a fuel element channel tube at the center of the reactor core

Gamma scanning was used to obtain activation profiles for each radioelement. Each object and each measurement configuration was modeled. Source terms were defined for each segment observed, with allowance for the imaging data. The contribution of each segment to each measuring point was then examined. The model gave an  $n \times n$  square matrix of transfer functions (number of measuring points  $\times$  number of segments) relating the activity and flux density for each energy according to the following expression:

$$A(E) = M^{-1}(E) \cdot F(E) \quad (\text{Eq. 1})$$

where  $A(E)$  is the activity vector ( $\text{GBq} \cdot \text{g}^{-1}$ ),  $M(E)$  the invertible matrix of transfer functions ( $\gamma \cdot \text{cm}^{-2} \cdot \text{s}^{-1} / \text{GBq} \cdot \text{g}^{-1}$ ) and  $F(E)$  the flux density vector ( $\gamma \cdot \text{cm}^{-2} \cdot \text{s}^{-1}$ ). Each term of the flux density vector is given by the following relation:

$$F(E) = \frac{N(E)}{t \cdot \Gamma(E) \cdot K(E)} \quad (\text{Eq. 2})$$

where  $N(E)$  is peak area of the spectrum (counts),  $t$  the counting time (s),  $\Gamma(E)$  the probability that the radionuclide emission will be of energy ( $E$ ) (dimensionless), and  $K(E)$  the absolute detector efficiency at energy ( $E$ ) ( $\text{cm}^2$ ).

If the radionuclide is a multiline  $\gamma$  emitter its activity  $A$  is determined as the mean of the calculated activities for each of the peaks  $A(E)$ , weighted by  $\sigma A(E)$ , the uncertainty on the corresponding peak.

**Fig. 3** shows the  $\gamma$  scanning results for a fuel element channel tube at the center of the core ( $^{60}\text{Co}$  flux density at detector level between  $1 \times 10^5$  and  $2 \times 10^7$   $\text{pH}\cdot\text{s}^{-1}\cdot\text{cm}^{-2}$ ).

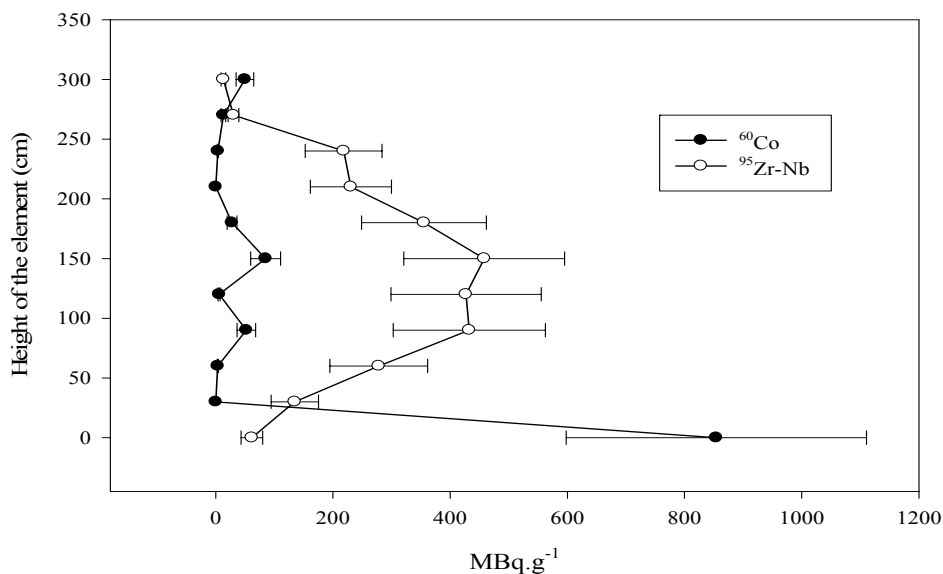


**Fig. 3.**  $\gamma$  scanning results for a fuel element channel tube centrally positioned in the reactor core

The figure identifies several activation products corresponding to the materials observed. The lower portion of the channel tube made of stainless steel and aluminum produces the high  $^{60}\text{Co}$  activity, while the Zircaloy central portion accounts for the  $^{95}\text{Zr-Nb}$  and  $^{125}\text{Sb}$  activity following an activation profile consistent with the shape of the neutron flux. The activity levels measured *in situ* are comparable to those measured on the samples analyzed in the laboratory. **Table II** compares the results of destructive and nondestructive analysis.

**Table II.** Comparison between destructive and nondestructive measurements on channel tube constituent materials

Samples	<i>In situ</i> measurements		Sample measurements	
	$^{65}\text{Zn}$ (MBq.g $^{-1}$ )	$^{60}\text{Co}$ (MBq.g $^{-1}$ )	$^{65}\text{Zn}$ (MBq.g $^{-1}$ )	$^{60}\text{Co}$ (MBq.g $^{-1}$ )
Aluminum	3 to 70	2 to 30	4 to 12	21 to 44
Stainless steel	DL	100 to 850	< 3	670 to 700

As for the reactor vessel, the close agreement between measured and calculated values validates the waste inventory predicted by the models, including for some pure  $\beta$  emitters via destructive measurements. For example, for Zircaloy activation the mean predicted  $^{95}\text{Zr-Nb}$  activity is about  $120 \text{ MBq}\cdot\text{g}^{-1}$  and the measured value about  $130 \text{ MBq}\cdot\text{g}^{-1}$ . Gamma imaging supplements the data by showing that the activation is highly localized on objects such as control rods or plugs. GeHP measurements revealed the presence of elements in smaller quantities (< 1% of the total spectrum) such as  $^{59}\text{Fe}$ .

## THREE TECHNICAL ASPECTS OF THE MEASUREMENT CAMPAIGNS

### Validating the results

This is a fundamental issue, as the results of nondestructive measurements are always based on hypotheses. The validation principle since the early 2000s [3] has been based on a comparison of measurements performed with independent detectors. In the case of the core internals, the components are characterized using three detectors and three different detection principles. Gamma spectrometry estimates the activation profiles for each radioelement, from which a model was developed where the measured activities constitute the source term. This model yields a calculated estimate of the dose rates at various points in space, which are then compared with uncollimated measurement data from a probe. Similarly, the dose rates estimated from  $\gamma$  camera images (the images are only produced by unscattered  $\gamma$ ) are compared with the computed dose rates without allowing for the dose buildup factor. The results are considered valid if the differences between the calculated and measured values are less than the measurement uncertainty. **Fig. 4** illustrates the validation of the results for the reactor vessel.

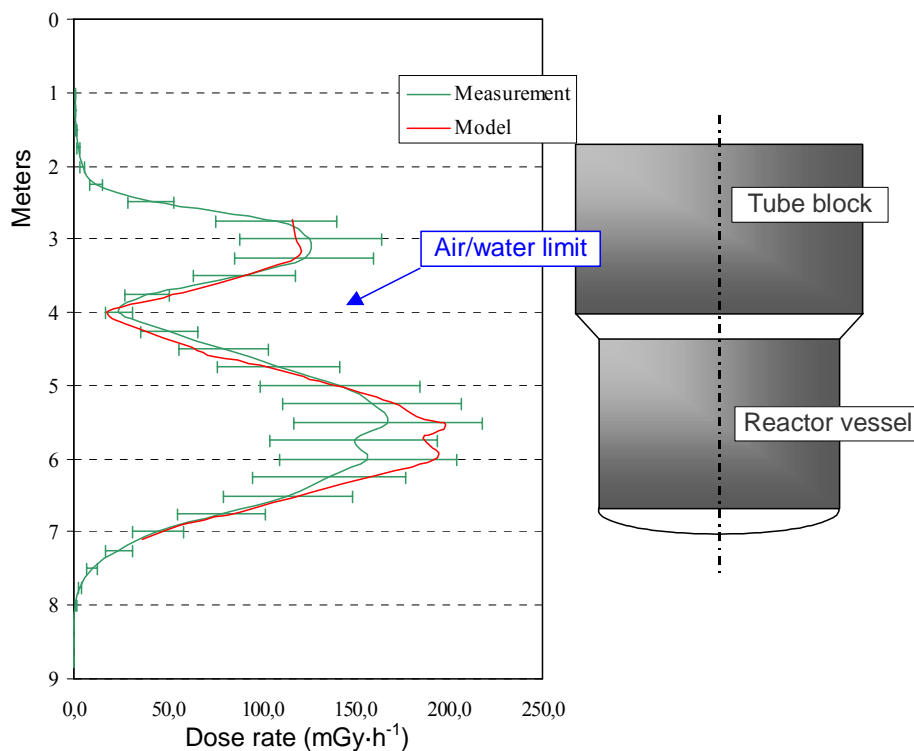


**Fig. 4.** Validation of the activation profile for the reactor vessel by comparison between predicted and measured dose rates

For this example the fit between the model and the measurement data is satisfactory, validating the activity estimate. The maximum deviation observed—less than 20%—is less than the mean uncertainty on the measured values (about 30%).

## Image analysis for modeling

The second technical contribution of these measurement campaigns concerns  $\gamma$  imaging to restrict the model hypotheses for estimating the activity. The core internals were measured in a radiologically clean environment (shielded cell) in which the only radioactive hot spots were on the objects observed. The activated zones on each component were identified on the  $\gamma$  images. By comparing them with the design drawings the main source terms were localized with relative accuracy. Using these findings as input data for the models substantially reduced the uncertainties on the predicted values.

The advantages of this combined approach are clearly illustrated in the case of the plugs. Like most of the internals, the plugs are roughly cylindrical objects about 3 meters high. On these components, however, only a single 30 cm<sup>3</sup> stainless steel part at the lower end was activated by the neutron flux. The images clearly show that the activation of the remainder of the plug is negligible. By referring to the drawings and comparing the radioelements identified by  $\gamma$  spectrometry the part responsible for the measured signal was pinpointed and taken into account as the only source term in the model. Without this additional information, the entire component section would have been considered as the source term. **Table III** illustrates the modeling error arising from the difference between the two hypotheses. In this example the geometric hypotheses are the same, only the term sources differ.

**Table III.** Effect of allowance for imaging data when modeling the estimated specific activity of reactor core plugs

Images taken into account		Images not taken into account	
<sup>60</sup> Co activity (GBq·g <sup>-1</sup> )	± 2σ	<sup>60</sup> Co activity (GBq·g <sup>-1</sup> )	± 2σ
1.42	0.43	0.27	0.08

## Coupling CdZnTe $\gamma$ spectrometry with GeHP $\gamma$ spectrometry

Another interesting result of these tests concerns the complementary aspects of different  $\gamma$  spectrometry results. Qualitatively the mean spectra measured by GeHP were confirmed for the major elements by CdZnTe measurements. **Table IV** illustrates this fit in the case of a regulating rod channel tube.

**Table IV.** Mean emerging  $\beta\gamma$  spectrum from a regulating channel tube rod measured by two different  $\gamma$  spectrometry systems

Detector	<sup>51</sup> Cr	<sup>46</sup> Sc	<sup>59</sup> Fe	<sup>65</sup> Zn	<sup>60</sup> Co
CdZnTe	14.1 ± 5.7%	–	–	41.1 ± 4.4%	44.8 ± 4.1%
GeHP	10.0% ± 1.1%	1.1% ± 2.1%	2.3% ± 1.8%	40.4% ± 0.8%	46.7 ± 0.6%

The discrepancies are attributable to the differences in the acquisition conditions (collimated and uncollimated measurements, different acquisition times, etc.) but only concern minor radioelements (< 2% of the mean spectrum).

This result was expected and has already been validated during intercomparison campaigns [4]. The additional advantage of the treatment described here is that it combines two measurements to estimate the activity of radioelements present in small quantities. Associating two detectors

allows the activity of these radioelements to be estimated by using the mean spectra measured with GeHP for low-irradiating elements and the activities measured by CdZnTe for highly irradiating elements. This is possible here because the objects were of the same composition and were activated under the same conditions.

## CONCLUSION

The measurement results discussed here illustrate the advantages of combining methods and techniques for *in situ* characterization of active components. Combining activation calculations, nondestructive measurements, and sample analyses provides an exhaustive and reliable inventory of the radionuclides affecting waste management. *In situ* measurements using a combination of multiple techniques (imaging, spectrometry, dose measurement) provide valuable data on the nature, level, and form of the source terms, while validating the results by comparison.

These measurements were carried out in a production reactor (between production campaigns) over a short period (about 1 month). This advanced knowledge will make it possible to prepare and reliably optimize the possible scenarios for future dismantling operations.

## REFERENCES

1. P. Gironès *et al.*, “Underwater Radiological Characterization of a Reactor Vessel”, ICEM'05, Glasgow, UK (2005).
2. C. Mahé *et al.*, “Imaging systems: new techniques for decommissioning”, DD&R Conf., Denver, CO, USA (2005).
3. C. Le Goaller *et al.*, “Association of innovative on-site measurement devices for characterization”, ICEM'05, Glasgow, UK (2005).
4. C. Le Goaller *et al.*, “In-Situ Nuclear Measurement for Decommissioning: Recent Trends and Needs”, IAEA, International Conference on Lessons Learned from Decommissioning of Nuclear Facilities and the Safe Termination of Nuclear Activities, Athens, Greece (2006).